Published in final edited form as:
Nat Geosci. 2018 ; 11: 77–81. doi:10.1038/s41561-017-0022-3.

Heterogeneous delivery of silicate and metal to the Earth by large planetesimals

S. Marchi[1,*], **R. M. Canup**[1], and **R. J. Walker**[2]

[1]Southwest Research Institute, Boulder, CO, USA.

[2]Deptartment of Geology, University of MD, College Park, MD, USA.

Abstract

After the Moon's formation, Earth experienced a protracted bombardment by leftover planetesimals. The mass delivered during this stage of late accretion has been estimated to be approximately 0.5% of Earth's present mass, based on highly siderophile element concentrations in the Earth's mantle and the assumption that all highly siderophile elements delivered by impacts were retained in the mantle. However, late accretion may have involved mostly large (≥ 1,500 km in diameter)—and therefore differentiated—projectiles in which highly siderophile elements were sequestered primarily in metallic cores. Here we present smoothed-particle hydrodynamics impact simulations that show that substantial portions of a large planetesimal's core may descend to the Earth's core or escape accretion entirely. Both outcomes reduce the delivery of highly siderophile elements to the Earth's mantle and imply a late accretion mass that may be two to five times greater than previously thought. Further, we demonstrate that projectile material can be concentrated within localized domains of Earth's mantle, producing both positive and negative ^{182}W isotopic anomalies of the order of 10 to 100 ppm. In this scenario, some isotopic anomalies observed in terrestrial rocks can be explained as products of collisions after Moon formation.

Models of the final stage of terrestrial planet formation envision large planetesimals (> 1,000 km in diameter) that were eventually removed by collisions or gravitational scattering over a timescale of up to a few 10^8 years[1]. The Moon is thought to be the result of a collision with the Earth by a ≥ 6,000-km-diameter projectile[2]. Evidence for continued accretion onto the Earth after the Moon's formation is found in the concentrations of highly siderophile elements (HSEs) in the Earth's mantle (for example, Re, Os, Ir, Ru, Pt, Rh, Pd and Au), which have strong chemical affinities for metallic iron. The mantle abundances of some HSEs are much higher than would result from metal–silicate equilibration during terrestrial

[*]**Correspondence and requests for materials** should be addressed to S.M. marchi@boulder.swri.edu.

Author contributions

S.M. conceived the work and analysed SPH results. R.M.C. performed SPH simulations and analysed the results. R.J.W. contributed HSE and W data and interpretation. All authors wrote the manuscript and discussed the results.

Competing interests

The authors declare no competing financial interests.

Methods

Methods, including statements of data availability and any associated accession codes and references, are available at https://doi.org/10.1038/s41561-017-0022-3.

Additional information

Supplementary information is available for this paper at https://doi.org/10.1038/s41561-017-0022-3.

core formation[3,4], and can be most easily explained by late accretion after core formation was complete[5,6].

Traditional estimates assume that HSEs delivered by late projectiles completely mixed and chemically equilibrated with Earth's mantle[7]. This may be true for undifferentiated projectiles, or for small, differentiated projectiles[8,9]. However, late projectiles may have been large and differentiated. Planetesimal size distributions consistent with the Moon-forming impactor imply multiple subsequent impacts with the Earth by 1,500- to 3,000-km-diameter projectiles (Methods). Comparably large projectiles have also been advocated to explain the relative abundances of HSEs on the Earth versus the Moon[10,11], and the origin of the Moon's orbital inclination[12]. Rocky planetesimals ≥ 1,500 km in diameter would probably have been differentiated (Methods). Portions of the projectile's core may then have merged with Earth's core, rather than being mixed into Earth's mantle[13], increasing the total late accretion mass needed to explain the observed mantle HSEs.

Partial accretion of differentiated planetesimals

We use smoothed-particle hydrodynamics (SPH) to simulate impacts into Earth by projectiles with masses (M_i) between 0.001 and 0.03 Earth masses ($M_\oplus$), corresponding to diameters ~1,400 to 4,400 km for a 4,000 kg m^{-3} density. The projectiles are differentiated with silicate mantles (70% by mass) and iron cores (30% by mass), which is similar to the average silicate-to-metal ratio for the terrestrial planets. For each projectile mass, we consider variable impact angles $\xi = 0°$, 30°, 45° and 60° ($\xi = 0°$ is a head-on impact), and variable impact velocities $v_i/v_e = 1.2$, 1.7 and 2.2 (~13, 19 and 24 km s^{-1}, respectively), where v_i is impact speed, v_e is the mutual escape velocity, while the median velocity expected during late accretion[1] is $v_i/v_e \sim 1.5$. Each simulation has $N = 2 \times 10^5$ to $N = 10^6$ SPH particles, and the projectile core is resolved by 400 to 2×10^3 particles.

A common outcome (Fig. 1) is that portions of the projectile's core are strongly decelerated by the initial impact and persist as coherent clumps many hundreds of kilometers across, even during temporary rebound soon after impact. This material originates predominantly from the interior and back side of the projectile's core that is farthest from the impact point. The largest clumps subsequently descend through the mantle, settling on Earth's core (Methods; Supplementary Fig. 1). These clumps are described by ≥ 10^2 SPH particles in our simulations, and their masses do not vary significantly with changes in SPH resolution (Methods). SPH cannot resolve small-scale turbulent mixing at the clump–mantle interface that could disrupt clumps during their descent[13,14]. However, at the time of late accretion, the Earth's mantle was predominantly or entirely solid (Methods). A solid mantle's high-viscosity makes turbulent erosion inefficient, implying that large clumps would survive (Methods; Supplementary Fig. 2).

We assume that all of a projectile's HSEs are within its core. As a result of the 'core crash effect' described above, and/or the escape of projectile core material, the delivery of HSEs to the Earth's mantle by large collisions can be disproportionate with their overall delivery of mass. To quantify this, we define three outcomes for projectile core particles at the end of our impact simulations: those that descend in large clumps to overlap with the target's core

particles ('core'); those that escape ('ejected'); and those that remain within the target's mantle or that are outside the planet but gravitationally bound ('mantle'). Projectile core material in the mantle at the end of our simulations has typically been stretched and dispersed during the impact, but has remained under pressure and is not vaporized. Turbulent erosion within local impact-produced melt pools (Supplementary Fig. 2) may further reduce this material to small size scales[9], allowing it to become oxidized[15] and mixed into the mantle. Core material lofted onto bound orbits is highly vaporized (~30 to 60% by mass), and may re-impact Earth as small condensates that efficiently equilibrate with the mantle[16].

Figure 2 shows the fate of projectile material as a function of projectile mass for $v_i/v_e = 1.7$ and $\xi = 30°$ and 45°. For the most probable impact angle $\xi = 45°$, ~20 to 40% of the projectile's core descends to the Earth's core and does not contribute to the mantle's HSE budget. In a similar fashion, ~0 to 60% of the projectile's core is ejected. For $v_i/v_e = 1.2/2.2$ higher/lower fractions of the projectile's core mergers with Earth's core. For highly oblique impacts with $\xi \geq 60°$, much or all of the projectile core escapes in all cases (Methods; Supplementary Fig. 3). For each projectile mass and impact velocity, we compute a characteristic fraction of projectile core retained in the Earth's mantle by averaging over the impact angle. This fraction ranges from 0.2 to 0.7 for $M_i = 0.001\ M_\oplus$, 0.2 to 0.6 for $M_i = 0.003\ M_\oplus$, 0.1 to 0.3 for $M_i = 0.01\ M_\oplus$ and 0.1 to 0.2 for $M_i = 0.03\ M_\oplus$, with variation for each mass due to increasing values of v_i/v_e. Generally similar averages are found even when the potential for escaping core material to later re-impact the Earth is included (Methods). The implication is that the late accreted mass delivered to Earth by large planetesimals may have been greater by a factor of about two to five compared with standard estimates, totalling ~0.01 to 0.03 $M_\oplus$. We note that late accretion impacts onto the Moon involved much smaller projectiles (≤ 200 km) than modelled here, that appear unlikely to undergo disproportionate accretion described above[9].

To assess the delivery of projectile silicate versus core to the terrestrial mantle, we define a delta-mass parameter (δM_t):

$$\delta M_t(\%) = \left[\left(M'_s/M'_m\right)/\left(M_s/M_m\right) - 1\right] \times 100$$

where M'_s and M'_m are the projectile silicate and metal mass delivered to Earth's mantle, respectively, while M_s and M_m are the bulk projectile silicate and metal mass, with $M_s/M_m = 2.33$. The value $\delta M_t = 0$ indicates that the projectile addition to the silicate Earth maintains the same silicate/metal proportion of the bulk projectile. Values of $\delta M_t > 0$ (< 0) indicate a disproportionate addition of silicate (metal). We find that large projectiles nearly always have $\delta M_t > 0$, even when accounting for projectile silicate that escapes (Fig. 2). This indicates that the mass delivered to the mantle by any one projectile tends to be disproportionately derived from the projectile's mantle. The integrated mass added to the mantle by large projectiles would then also be biased toward the silicate portions of these bodies, even if some of the projectiles were small and/or undifferentiated.

Impact-produced heterogeneous mantle domains

Our simulations show that the spatial distribution of projectile material within the Earth's mantle is often non-uniform, and as such large collisions could generate chemical and isotopic heterogeneities in the mantle with respect to the bulk silicate Earth. If such heterogeneities are of sufficient magnitude, and if subsequent mantle mixing is sufficiently slow and/or incomplete, they may ultimately be preserved in the rock record. To quantify such effects, we identify mantle domains with the highest concentrations of projectile material at the end of our SPH simulations (Fig. 3). We identify two endmember distributions of projectile material. In the first, an oblique impact produces a localized concentration of projectile core in typically mid to deep regions of the Earth's mantle (Fig. 3a,b). In the second, a more head-on collision deposits a large fraction of projectile's mantle in a near-surface spherical cap with a diameter of ~4,000 to 8,000 km, and a radial thickness of ~300 km (Fig. 3c,d).

Substantial concentrations of projectile materials within discrete mantle domains would affect the isotopic composition of these domains in tungsten (W), a moderately siderophile element. The variance in $\mu^{182}W$ (where $\mu^{182}W$ is the deviation in parts per million of the $^{182}W/^{184}W$ of a sample compared with a standard representing the modern, ambient terrestrial mantle) resulting from radioactive decay of ^{182}Hf ($t_{½}$ = 9 Myr), is commonly used to investigate the timing of core formation[17]. Well-resolved isotopic heterogeneities in W are measured in some terrestrial mantle-derived rocks[18–22]. The preservation of such signatures over billions of years indicates that mixing in the Earth's mantle has been incomplete. Prior works suggest that some W heterogeneities originated either by metal–silicate or silicate–silicate fractionation of Hf/W during Earth's primary stage of accretion[19,21]. This requires that the heterogeneities were preserved during the Moon-forming impact, implying that this event did not homogenize the Earth's mantle, a potentially problematic requirement for high-energy Moon-forming scenarios[23–25].

We propose that some heterogeneities might instead have been produced after the Moon-forming impact, during late accretion, when projectiles were smaller and limited mixing was perhaps more probable.

To estimate the W isotopic composition for domains identified with our SPH simulations as having enhanced projectile material (Fig. 3), we perform mass balance calculations assuming limited subsequent mixing, with isotopic and concentration parameters defined in the Methods section.

Figure 4a shows results for oblique impacts (ξ = 30° and 45°) that produce concentrated regions of projectile metal of mass $M_{p,m}$. Subsequent mixing of this material into a deep silicate Earth domain of mass $M_{e,s} \sim 10^2$ to 700 $M_{p,m}$ can produce $\mu^{182}W$ values of about −10 to −100 ppm (see Supplementary Table 1; Methods). Projectile metal would be rich in HSEs, and so such regions should nominally be enriched in HSEs too, even in the limiting case of a domain that had not previously received any HSEs during late accretion (Supplementary Table 1). The only currently known ancient terrestrial rocks with negative tungsten anomalies (the 3.55 Ga Schapenburg komatiites) are characterized by average

values of $\mu^{182}W$ of about −8 (ref. [20]), broadly consistent with our core-mixing scenario. However, the mantle source of these komatiites was estimated to be HSE depleted, rather than enriched. This is in disagreement with a single-step late accretion origin, although it is possible that HSE depletion could be produced through a secondary, partial silicate–metal differentiation event. Negative anomalies of values of $\mu^{182}W$ as low as −15 in some modern plume-derived ocean island basalts[26] might be better explained by this process.

A positive tungsten anomaly can be produced by a concentration of projectile mantle, whose strongly positive $\mu^{182}W$ value reflects the projectile's own earlier differentiation. Figure 4b shows results for relatively low-velocity, head-on impacts ($\xi = 0°$ and 30°), which have no or few projectile core particles in the region of projectile mantle concentration, whose mass is $M_{p,s}$. If subsequent mixing occurs across an Earth mantle domain of mass $M_{e,s}$ of a few to 10 $M_{p,s}$, resulting anomalies have $\mu^{182}W$ of about +50 to +200 ppm, depending on the projectile size. Higher impact speeds and/or more grazing collisions ($\xi \sim 45–60°$) result in generally smaller positive anomalies, of the order of 10 ppm. For example, supracrustal rocks from Isua, Greenland (~3.7 Ga) have average values[18,27,28] of $\mu^{182}W$ of about +13. It has been suggested that the positive anomalies reflect derivation from portions of the Earth's mantle isolated from some portion of late accretionary additions[18]. This would be accompanied by variable depletion in HSE compared with the modern mantle. Estimates of the abundances of HSE in the mantle sources of these rocks range from ~50 to 100% of modern concentrations[27,28]. Our mixing model can simultaneously account for both the positive W isotopic anomalies and the HSE concentrations of these and other early Earth supracrustal rocks by considering a late impact into a mantle that has already received most of its HSEs from prior late accretion delivery (see Supplementary Table 1; Methods). The mixing scenarios presented above represent the easiest ways our model could produce mixing compatible with some observed W data, and other scenarios are also possible.

Variation in large impact characteristics and in the timing of such impacts during the late accretion epoch can thus lead to regions with either positive or negative $\mu^{182}W$ anomalies and a range of HSE abundances. If observed ^{182}W anomalies are the result of late accretion, their properties could provide new constraints on the magnitude and timing of early terrestrial collisions.

Methods

Late accretion projectile size–frequency distribution.

The size distribution of late accreted planetesimals is uncertain. Dynamical models suggest that during the final stage of terrestrial planet accretion, half or more of the initial mass was contained in Moon-sized and larger objects, with the remainder contained in smaller bodies (see, for example, refs [1,29,30]). Such simulations do not typically resolve the formation of lunar- and sub-lunar-sized bodies. However, the simulations can be used to constrain the decay rate of the bombardment produced by such remnants, which is estimated to decrease to ~10% of its initial rate in approximately 50 Myr (ref. [31]).

As a simple estimate of the likelihood of projectiles ≥ 1,500 km in diameter hitting the Earth after the Moon-forming impact, we consider a power-law size distribution of planetesimals

with $dN_b \propto R^{-q}\,dr$, where dN_b is the number of bodies with radii between R to $R + dR$ and q is a differential size index. We consider that at the time of the Moon-forming impact, the postulated Mars-sized projectile was the largest member of such a distribution in the Earth's vicinity, so that $N_b(>R_{gi}) = 1$, where $R_{gi} \sim 3{,}500$ km is the radius of the giant impactor, and that the planetesimal size distribution had most of its mass in its largest bodies, implying $q < 4$. The number of bodies with radius greater than R expected to impact the Earth before this population was greatly diminished (that is, within the first few 10^7 to 10^8 years after the Moon formed) would be of the order of $(R_{gi}/R)^{q-1}$. For $2 \leq q \leq 3.5$, this implies between 5 and 50 projectiles > 1,400 km in diameter (that is, with masses > 0.001 $M_\oplus$), and between 2 and 8 projectiles > 3,000 km in diameter (with masses > 0.01 $M_\oplus$). Thus, multiple impacts by projectiles in the size range we consider here are likely.

Several other independent arguments have been made for such large projectiles during late accretion as a means to explain: the disproportionate accretion of HSEs onto the Earth versus the Moon (also strengthened by the offset in ^{182}W isotopic composition between the lunar and terrestrial mantles[10,11,32,33]); the Moon's heavily cratered terrains[31,34]; and the origin of the Moon's orbital inclination through gravitational scattering[12].

Differentiation state of large projectiles.

The energy per unit mass of accreting a uniform density body of mass M and radius R is $E_{acc} = (3/5)GM/R$. For the projectiles we consider, $0.001 \leq M\,(M_\oplus) \leq 0.03$, $700 \leq R\,(\text{km}) \leq 2{,}200$, and $3.4 \times 10^9 \leq E_{acc}\,(\text{erg g}^{-1}) \leq 3.3 \times 10^{10}$. For specific heat $C \sim 8 \times 10^6$ erg g^{-1} K^{-1}, the average temperature rise due to accretional heating alone is $400 \leq \Delta T\,(\text{K}) \leq 4{,}000$ in the limit of no radiative cooling. As accretional energy is expected to be deposited at depth in the target, cooling is inefficient unless the object is partially or fully molten; as a result, large objects tend to retain the heat of their formation until they begin to melt (see, for example, ref. [35]). Accretional heating alone would thus have probably melted projectiles with $M \geq 0.005\ M_\oplus$. Heating from ^{26}Al radiogenic decay may have also occurred. If a projectile formed in $\leq 2 \times 10^6$ yr, which is plausible for the projectile sizes we consider[36], the average temperature rise due to ^{26}Al heating would be ≥ 1,000 K (see, for example, ref. [37] and values therein). The combination of accretional and radiogenic heating may thus have heated all of the projectiles we consider to temperatures high enough for melting and internal differentiation into rocky mantles and metallic cores. For comparison, Vesta, known to be a differentiated rocky body, is 20 times less massive than the smallest projectile here.

Re-accretion of ejected projectile core material.

A primary goal of this work is to estimate the fraction of a large projectile's core that remains in the Earth's mantle (M'_m/M_m). For a given characteristic projectile mass and velocity, the total late accreted mass needed to account for terrestrial mantle HSE concentrations is approximately $(0.005\ M_\oplus)/\langle M'_m/M_m\rangle$, where a late accretion mass of 0.005 $M_\oplus$ corresponds to traditional estimates that assume $M'_m/M_m = 1$, and $\langle M'_m/M_m\rangle$ is the angle-averaged value derived from our SPH simulations.

In the main text, we estimate (M'_m/M_m) by including both core particles that remain within the target's mantle at the end of our SPH simulations and particles launched into bound

orbits that may later re-impact the Earth. Here we consider, in addition, projectile core particles that escape but that may later re-impact the Earth and thereby increase (M'_m/M_m).

The efficiency of re-impact depends on ejecta particle size. The fraction of large bodies ejected from Earth on heliocentric orbits that will re-impact Earth is f_{imp} ~ 0.3 to 0.45 (refs [38,39]). Small fragments will undergo mutually destructive collisions and be ground away before they re-impact[38,39]. Intermediate sizes are partly removed by re-impact and partly by collisional grinding. In Fig. 10 of ref. [38], it is estimated that the fraction of ejecta removed by collisional grinding is f_{grind} = 0.5 for 100-km-scale ejecta, f_{grind} = 0.9 for 10-km scale ejecta, and f_{grind} ~ 1 for vaporized ejecta, because this material re-condenses to very small particle sizes that are rapidly removed by radiation forces.

We use these results to estimate the portion of the escaping projectile core mass that will re-impact Earth and add metal to the terrestrial mantle for each of our SPH simulations. In most cases, escaping core particles are dispersed and described by individual SPH particles on diverging trajectories (for example, all cases in Fig. 2). The ejecta particle sizes are then not resolved; they would be no more massive than an individual SPH particle (equivalent to a ~100 km body), but could well be much less massive/smaller. For these cases, we calculate the vapour fraction of the escaping core particles, f_{vap}, using ANEOS[40]. Typical values are tens of per cent vapor by mass. We then estimate the mass of escaping core particles that will re-impact Earth and be incorporated into its mantle as $M_{acc} \sim (1-f_{vap})(f_{imp})(1-f_{grind})M_{esc}$, where M_{esc} is the total escaping core mass, and we set f_{imp} = 0.4 and f_{grind} = 0.9 or 0.5, corresponding to 10-km- or 100-km-scale ejecta fragments.

In highly oblique (≥ 60°) collisions (for example, Supplementary Fig. 3), escaping material is contained primarily in a large differentiated object. In these cases, we estimate the mass of core particles that would re-impact the Earth and add metal to the Earth's mantle as $M_{acc} = (f_{imp})\langle M'_m/M_m\rangle M_{esc}$, with $\langle M'_m/M_m\rangle$ determined from our SPH simulations of impacts of the parent projectile at various impact angles. Here, f_{imp} accounts for the likelihood that the large body will re-impact Earth, and $\langle M'_m/M_m\rangle$ approximates the portion of the large body's core that will end up in the mantle following re-impact. The latter is approximate because the core-to-mantle ratio in the re-impacting ejected body is different from that in our simulated projectiles.

For all of our projectile masses and impact velocities, M_{acc} is negligible for 0 or 30° impact angles. For 45° cases, M_{acc} is typically a few to 10% of M'_m, so that the mass of metal delivered to the mantle would be minimally increased by re-impacting ejecta. The largest effect is for impact angles ≥ 60°, because in these cases the escaping mass is large, and typically some tens of per cent of the ejected core material may re-impact the Earth and be retained in the mantle.

To quantify the effect of metal re-impact for each projectile mass and impact velocity, we compute an angle-averaged value, $\langle M'_m/M_m\rangle^*$, that includes the contribution of M_{acc} and compare this with the $\langle M'_m/M_m\rangle$ value computed without this contribution. In the limiting case that dispersed non-vaporized material is contained in 100 km bodies, $\langle M'_m/M_m\rangle^*$ differs from $\langle M'_m/M_m\rangle$ by several tens of per cent for the largest projectiles (0.03 $M_\oplus$), and

by 10 to 15% for smaller projectiles. We consider it likely that ejecta particles were much smaller than this. For 10 km ejecta, $<M'_m/M_m>^*$ differs by a few to 10% from $<M'_m/M_m>$ for all cases; smaller ejecta sizes yield even smaller differences. Thus, re-impact of escaping metal appears unlikely to affect our basic conclusion in the main text that the late accreted mass may have been a factor of two to five larger than previously thought.

Impact simulations.

Collisions by projectiles much smaller than the target are often modelled using Eulerian (grid-based) hydrocodes that treat the target as an infinite plane (for example, ref. [9]). For large impacts, such as those in which the projectile and the target sizes differ by less than a factor of ten, the target's shape and the self-gravity of the impactor and target as they are distorted by the collision are important, and a numerical treatment that includes both is desirable. Our code[2] implements the equation of state M-ANEOS[40], and includes explicit self-gravity. The energy budget is determined by shock dissipation, and work done by compressional heating and expansional cooling; material strength is ignored. Particle smoothing lengths within the target and impactor are $h \sim 10^2$ km. While SPH may aptly track the overall dynamical outcome of a large impact, as well as flow regions described by many SPH particles, fluid behaviour at scales comparable to or smaller than h is not treated by SPH.

Supplementary Fig. 1 shows the behaviour of a projectile's core in a 10^6-particle simulation. For an average 45° impact angle, large iron clumps form preferentially from material initially located in the mid back side of the projectile's core, with front–back defined by the approach trajectory. The front portions of the core impact first, and there is then a 'pile-up' effect as the rear portions collide with the front portions. The net effect is that a region of inner core material ends up temporarily at rest and non-dispersed in the very early stages of the collision (Supplementary Fig. 1a). This creates favourable conditions for the formation of clumps that then accelerate downward toward the target's centre (Supplementary Fig. 1b–d). For the average 45° impact angle, lower impact velocities tend to preserve a larger part of the core intact that is more efficiently delivered to the core–mantle boundary, while higher impact velocities result in more core dispersal and reduced delivery to the Earth's core–mantle boundary.

We conducted a resolution test of a single 45° collision in which the number of SPH particles in the projectile was varied by a factor of 25 across three simulations (from $\sim 2 \times 10^2$ to 6×10^3). The three runs yielded broadly similar large clump masses and a similar fraction of the impactor core that descends to the core–mantle boundary.

Turbulent erosion of clumps.

Two key simplifications in SPH models must be considered when interpreting results from our simulations. First, although our SPH model treats phase transitions in a thermodynamically consistent manner, it does not include strength or internal friction associated with partial or complete solidification. In this respect, the code treats objects as fluid gravitating bodies. Second, SPH cannot treat behaviour that occurs on a spatial scale that is comparable to or smaller than an individual SPH particle. This would include

turbulence along the interface between the terrestrial mantle and the surfaces of large descending clumps of projectile core material. Such turbulence could erode clumps, depending on the clump size and the distance clumps descend through a fluid, low-viscosity magma (see, for example, refs [13,14,41]).

Immediately after the Moon-forming impact, the Earth's mantle would have been primarily-to-fully molten (see, for example, ref. [42]). Magma oceans on Earthsized planets are unlikely to form conductive lids, so that their subsequent rate of cooling would be regulated by thermal blanketing by a volatile-rich atmosphere (see, for example, refs [43,44]). Models accounting for such effects suggest that 98% of Earth's mantle would have solidified within 5 Myr after the Moon-forming impact[43,45,46]. Complete solidification of the shallow magma ocean requires ~10^7 to 10^8 yr (ref. [47]). The timing of large, late accretionary impacts is uncertain, but dynamical simulations suggest that the timescale for depletion of 90% of leftover planetesimals is of the order of 50 Myr, while a long-lived tail of collisions could last for several hundred million years (refs [11,31]). Thus, the collisions considered in this work occur after the magma ocean resulting from the Moon formation had essentially solidified and any remnant magma ocean—if present—was very shallow. Heating from the impact itself melts a local region of mantle (Supplementary Fig. 2), but below this melt pool the post-impact mantle is expected to be sub-solidus.

For the impact in Fig. 1, the largest two clumps have widths of ~600 and ~400 km (note that in our images we plot a point at the centre of each SPH particle, when in reality each SPH particle represents material distributed across a diameter of roughly twice its smoothing length). These clumps tend to initially form near the bottom of the impact-induced melt pool (Supplementary Fig. 2). As a result of this, and because any remnant magma ocean at the time of late accretion is expected to be very shallow if present at all, we expect the clumps descend through a localized fluid magma layer that is smaller than their diameter. Analytical fluid dynamical models and laboratory experiments suggest that there would be minimal clump erosion in such a circumstance[13].

Below the local melt pool, crystallization increases the mantle viscosity greatly (by 10 to 20 orders of magnitude) compared with that in a fluid mantle (see, for example, ref. [47]). Descent through a solid mantle would then be characterized by vastly less effective turbulence, and diffusive equilibrium between the silicate and metal would be inhibited by the very low solid diffusivity[13]. Detailed models suggest that large liquid metal diapirs descend through a solid mantle to the core–mantle boundary via Stokes flow[48–50]. This is consistent with our overall picture here, although the rapid descent of large clumps seen in the SPH simulations would in reality occur with a velocity that depends on viscosity (see, for example, ref. [48]).

It is also worth noting that metal stranded in the mantle at the end of our simulations could still reach the core, for example because stressed partially molten silicates will provide pathways for percolation of iron (see, for example, ref. [51]). A detailed exploration of this is left for future work.

Mixing calculations.

We implemented two-component isotopic mixing, using the following formula:

$$\mu^{182}W_{mix} = \left(\mu^{182}W_1 + 1\right)(1 + gf\gamma)/(1 + gf) - 1$$

where $f = {}^{184}W_2/{}^{184}W_1$, $g = M_2/M_1$ and $\gamma = (\mu^{182}W_2 + 1)/(\mu^{182}W_1 + 1)$. M and W indicate the mass and tungsten weight per cent abundances of each component, respectively. Note that for two-component mixing, it is the ratio of the absolute W concentration (f) that matters, along with the mass ratio (g). For this, we adopt $\mu^{182}W$ values of −250 and + 2,000, respectively, for the metal and silicate fractions of the projectiles. We also assume W concentrations of 500 and 6 ppb, and Pt concentrations of 5,700 and 0.1 ppb, respectively, for the core and mantle of the projectile. These values are justified by typical compositions of iron and achondrite meteorites (see, for example, ref. [17]). Note that our assumptions imply a bulk projectile $\mu^{182}W_{mix} = -188$, corresponding to average chondritic meteorites. We have also explored non-chondritic projectile compositions, and find that the ability of heterogeneous projectile delivery to generate significant W isotopic anomalies is largely unaffected by the specific $\mu^{182}W$ and W values used for the projectile's core and mantle.

For mixing of projectile core and terrestrial mantle, we envision addition of the metal to a deep mantle domain that is devoid of a prior late accretionary addition. For this scenario, W and Pt concentrations of 15 and 0.1 ppb are assumed for the terrestrial mantle, respectively. We also assume a pre-late accretionary $\mu^{182}W$ value for this mantle to be +26 (refs [32,33]).

For mixing of projectile mantle with terrestrial mantle, we consider impacts occurring after ~80% of late accretion to the terrestrial mantle is complete ($\mu^{182}W = +5$, Pt = 7 ppb), and that the previously late accreted materials are well mixed through the mantle. In contrast to the addition of projectile metal, the addition of projectile mantle has only a dilutional effect on HSE concentrations in the resulting mixture. Consequently, calculated Pt concentrations in the mixtures are broadly similar to that in the current bulk silicate Earth (Supplementary Table 1) and consistent with measured levels in the positive W-anomaly terrestrial samples[27].

Our parameter choices are motivated by explaining both negative and positive ^{182}W anomalies. If one assumes a fixed terrestrial reservoir (that is, corresponding to a fixed time during late accretion), then one cannot explain both positive and negative anomalies with any combination of impactor material. However, there would have generally been a temporal evolution of conditions seen by late accretionary projectiles, with negative anomalies produced early before late accretion of HSE, while positive anomalies can be produced late. It should be noted that positive and negative W anomalies can also be attained regardless of the temporal evolution of the mantle, and the scenario presented above is invoked to also explain HSE abundances of observed samples.

Supplementary Table 1 reports mixing results as in Fig. 4. M'_m, M'_s and M_s are projectile metal and silicate, and Earth silicate, respectively. Negative anomalies: $\mu^{182}W$ Mix 1–2 indicates $M'_m + M_s$ two-component mixing calculations. We used W abundances of 500 and

15 ppb for projectile core and Earth silicate, respectively. This corresponds to a mixing ratio of ~3% (our nominal model in Fig. 4a). μ^{182}W Mix 1–2–3 indicates three-component mixing calculations. Here we used a W abundance of 6 ppb for projectile silicate and 15 ppb for $M'_{m} + M_{s}$. This shows that the addition of projectile silicate material has a negligible effect. Positive anomalies: μ^{182}W Mix 1–2 indicates $M'_{s} + M_{s}$ two-component mixing calculations. We used W abundances of 6 and 15 ppb for projectile and Earth silicate, respectively. This corresponds to a mixing of ~71% (our nominal model in Fig. 4b). μ^{182}W Mix 1–2–3 indicates three-component mixing calculations. For this, we used 15 ppb for $M'_{s} + M_{s}$ and 500 ppb for M'_{m}. As shown, the addition of projectile metal is negligible in most cases. In rare instances, a few metal particles remain close to the surface and may result in slightly negative anomalies (with respect to +26). For both cases, we also report the Pt concentrations resulting from the two-component mixing.

The current Earth–Moon difference in tungsten isotopic composition is traditionally interpreted as a result of their having identical μ^{182}W values immediately after the Moon-forming impact, followed by a chondritic late accretion that disproportionately reduced Earth's value (see, for example, ref. [33]). For large impacts, preferential incorporation of impactor mantle would lead to the preferential addition of ^{182}W to the mantle, compared with a bulk chondritic addition. How such a non-chondritic late accretion would affect the evolution of Earth–Moon tungsten compositions is a topic for future work.

Code availability.

The SPH code is not available. An IDL W mixing code is available upon request.

Data availability.

Binary file outputs of SPH impact simulations are available upon request.

Supplementary Material

Refer to Web version on PubMed Central for supplementary material.

Acknowledgements

We thank F. Nimmo, K. Pahlevan, D. Stevenson and A. Morbidelli for discussion and comments that greatly improved the paper. S.M. and R.M.C. thank NASA Exobiology grant NNX15AL26G and NASA SSERVI programmes for support. R.J.W. acknowledges NASA Emerging Worlds grant NNX16AN07G, and NASA SSERVI grant NNA14AB07A.

References

1. Raymond SN, Schlichting HE, Hersant F & Selsis F Dynamical and collisional constraints on a stochastic late veneer on the terrestrial planets. Icarus 226, 671–681 (2013).
2. Canup RM Simulations of a late lunar-forming impact. Icarus 168, 433–456 (2004).
3. Mann U, Frost DJ, Rubie DC, Becker H & Audétat A Partitioning of Ru, Rh, Pd, Re, Ir and Pt between liquid metal and silicate at high pressures and high temperatures — implications for the origin of highly siderophile element concentrations in the Earth's mantle. Geochim. Cosmochim. Acta 84, 593–613 (2012).

4. Rubie DC et al. Accretion and differentiation of the terrestrial planets with implications for the compositions of early-formed Solar System bodies and accretion of water. Icarus 248, 89–108 (2015).
5. Kimura K, Lewis RS & Anders E Distribution of gold and rhenium between nickel-iron and silicate melts: implications for the abundance of siderophile elements on the Earth and Moon. Geochim. Cosmochim. Acta 38, 683–701 (1974).
6. Chou C-L. Fractionation of siderophile elements in the Earth's upper mantle; Proc. 9th Lunar and Planetary Science Conference; 1978. 219–230.
7. Walker RJ Highly siderophile elements in the Earth, Moon and Mars: update and implications for planetary accretion and differentiation. Chem. Erde 69, 101–125 (2009).
8. Rubie DC, Melosh HJ, Reid JE, Liebske C & Righter K Mechanisms of metal-silicate equilibration in the terrestrial magma ocean. Earth Planet. Sci. Lett 205, 239–255 (2015).
9. Kendall JD & Melosh HJ Differentiated planetesimal impacts into a terrestrial magma ocean: fate of the iron core. Earth Planet. Sci. Lett 448, 24–33 (2016).
10. Bottke WF, Walker RJ, Day JMD, Nesvorny D & Elkins-Tanton L Stochastic late accretion to Earth, the Moon, and Mars. Science 330, 1527–1530 (2010). [PubMed: 21148387]
11. Marchi S et al. Widespread mixing and burial of Earth's Hadean crust by asteroid impacts. Nature 511, 578–582 (2014). [PubMed: 25079556]
12. Pahlevan K & Morbidelli A Collisionless encounters and the origin of the lunar inclination. Nature 527, 492–494 (2015). [PubMed: 26607544]
13. Dahl TW & Stevenson DJ Turbulent mixing of metal and silicate during planet accretion — and interpretation of the Hf–W chronometer. Earth Planet. Sci. Lett 295, 177–186 (2010).
14. Deguen R, Landeau M & Olson P Turbulent metal-silicate mixing, fragmentation, and equilibration in magma oceans. Earth Planet. Sci. Lett 391, 274–287 (2014).
15. Wade J & Wood BJ Core formation and the oxidation state of the Earth. Earth Planet. Sci. Lett 236, 78–95 (2005).
16. Kraus RG et al. Impact vaporization of planetesimal cores in the late stages of planet formation. Nat. Geosci 8, 269–272 (2015).
17. Kleine T et al. Hf–W chronology of the accretion and early evolution of asteroids and terrestrial planets. Geochim. Cosmochim. Acta 73, 5150–5188 (2009).
18. Willbold M, Elliott T & Moorbath S The tungsten isotopic composition of the Earth's mantle before the terminal bombardment. Nature 477, 195–198 (2011). [PubMed: 21901010]
19. Touboul M, Puchtel IS & Walker RJ ^{182}W evidence for long-term preservation of early mantle differentiation products. Science 335, 1065–1069 (2012). [PubMed: 22345398]
20. Puchtel IS, Blichert-Toft J, Touboul M, Horan MF & Walker RJ Coupled ^{182}W–^{142}Nd record of the early differentiation of Earth's mantle. Geochem. Geophys. Geosyst 17, GC006324 (2016).
21. Rizo H et al. Memories of Earth formation in the modern mantle: W isotopic compositions of flood basalt lavas. Science 352, 809–812 (2016). [PubMed: 27174983]
22. Willbold M, Mojzsis SJ, Chen H-W & Elliott T Tungsten isotope composition of the Acasta Gneiss Complex. Earth Planet. Sci. Lett 419, 168–177 (2015).
23. Ćuk M & Stewart ST Making the Moon from a Fast-Spinning Earth: A Giant Impact Followed by Resonant Despinning. Science 338, 1047–1052 (2012). [PubMed: 23076099]
24. Canup RM Forming a Moon with an Earth-like composition via a giant impact. Science 338, 1052–1055 (2012). [PubMed: 23076098]
25. Nakajima M & Stevenson DJ Melting and mixing states of the Earth's mantle after the Moon-forming impact. Earth Planet. Sci. Lett 427, 286–295 (2015).
26. Mundl A et al. Tungsten-182 heterogeneity in modern ocean island basalts. Science 356, 66–69 (2017). [PubMed: 28386009]
27. Rizo H et al. Early Earth differentiation investigated through ^{142}Nd, ^{182}W, and highly siderophile element abundances in samples from Isua, Greenland. Geochim. Cosmochim. Acta 175, 319–336 (2016).

28. Dale CW, Kruijer TS & Burton KW Highly siderophile element and ^{182}W evidence for a partial late veneer in the source of 3.8 Ga rocks from Isua, Greenland. Earth Planet. Sci. Lett 458, 394–404 (2017).
29. O'Brien DP, Morbidelli A & Levison HF Terrestrial planet formation with strong dynamical friction. Icarus 184, 39–58 (2006).
30. Jacobson SA & Morbidelli A Lunar and terrestrial planet formation in the Grand Tack scenario. Phil. Trans. R. Soc. A 372, 0174 (2014).
31. Morbidelli A, Marchi S, Bottke WF & Kring DA A sawtooth-like timeline for the first billion years of lunar bombardment. Earth Planet. Sci. Lett 355–356, 144–151 (2012).
32. Touboul M, Puchtel IS & Walker RJ Tungsten isotopic evidence for disproportional late accretion to the Earth and Moon. Nature 520, 530–533 (2015). [PubMed: 25855299]
33. Kruijer TS, Kleine T, Fischer-Gödde M & Sprung P Lunar tungsten isotopic evidence for the late veneer. Nature 520, 534–537 (2015). [PubMed: 25855296]
34. Marchi S, Bottke WF, Kring DA & Morbidelli A The onset of the lunar cataclysm as recorded in its ancient crater populations. Earth Planet. Sci. Lett 325, 27–38 (2012).
35. Pritchard ME & Stevenson DJ in Origin of the Earth and Moon (eds Canup RM & Righter K) 179 (Univ. Arizona Press, Tuscon, 2000).
36. Levison HF, Kretke KA, Walsh KJ & Bottke WF Growing the terrestrial planets from the gradual accumulation of sub-meter sized objects. Proc. Natl Acad. Sci. USA 112, 14180–14185 (2015). [PubMed: 26512109]
37. Barr AC & Canup RM Origin of the Ganymede–Callisto dichotomy by impacts during the late heavy bombardment. Nat. Geosci 3, 164–167 (2010).
38. Jackson AP & Wyatt MC Debris from terrestrial planet formation: the Moon-forming collision. Mon. Notices Royal Astron. Soc 425, 657–679 (2012).
39. Bottke WF et al. Dating the Moon-forming impact event with asteroidal meteorites. Science 348, 321–323 (2015). [PubMed: 25883354]
40. Melosh HJ A hydrocode equation of state for SiO2. Meteorit. Planet. Sci 42, 2079–2098 (2007).
41. Wacheul J-B, Le Bars M, Monteux J & Aurnou JM Laboratory experiments on the breakup of liquid metal diapirs. Earth Planet. Sci. Lett 403, 236–245 (2014).
42. Canup RM Lunar-forming collisions with pre-impact rotation. Icarus 196, 518–538 (2008).
43. Elkins-Tanton LT Magma oceans in the inner solar system. Annu. Rev. Earth Planet. Sci 40, 113–139 (2012).
44. Zahnle KJ, Lupu R, Dobrovolskis A & Sleep NH The tethered Moon. Earth Planet. Sci. Lett 427, 74–82 (2015).
45. Elkins-Tanton LT Linked magma ocean solidification and atmospheric growth for Earth and Mars. Earth Planet. Sci. Lett 271, 181–191 (2008).
46. Hamano K, Abe Y & Genda H Emergence of two types of terrestrial planet on solidification of magma ocean. Nature 497, 607–610 (2013). [PubMed: 23719462]
47. Solomatov VS in Treatise on Geophysics Vol. 9 (ed. Schubert G) 91–120 (Elsevier, Heinrich, 2007).
48. Samuel H A re-evaluation of metal diapir breakup and equilibration in terrestrial magma oceans. Earth Planet. Sci. Lett 313, 105–114 (2012).
49. Stevenson DJ in Origin of the Earth (ed. Jones H.E.N.a.J.H.) 231–250 (Oxford University Press, New York, 1990).
50. King C & Olson P Heat partitioning in metal-silicate plumes during Earth differentiation. Earth Planet. Sci. Lett 304, 577–586 (2011).
51. Zimmerman ME, Zhang S, Kohlstedt DL & Karato S-I Melt distribution in mantle rocks deformed in shear. Geophys. Res. Lett 26, 1505–1508 (1999).

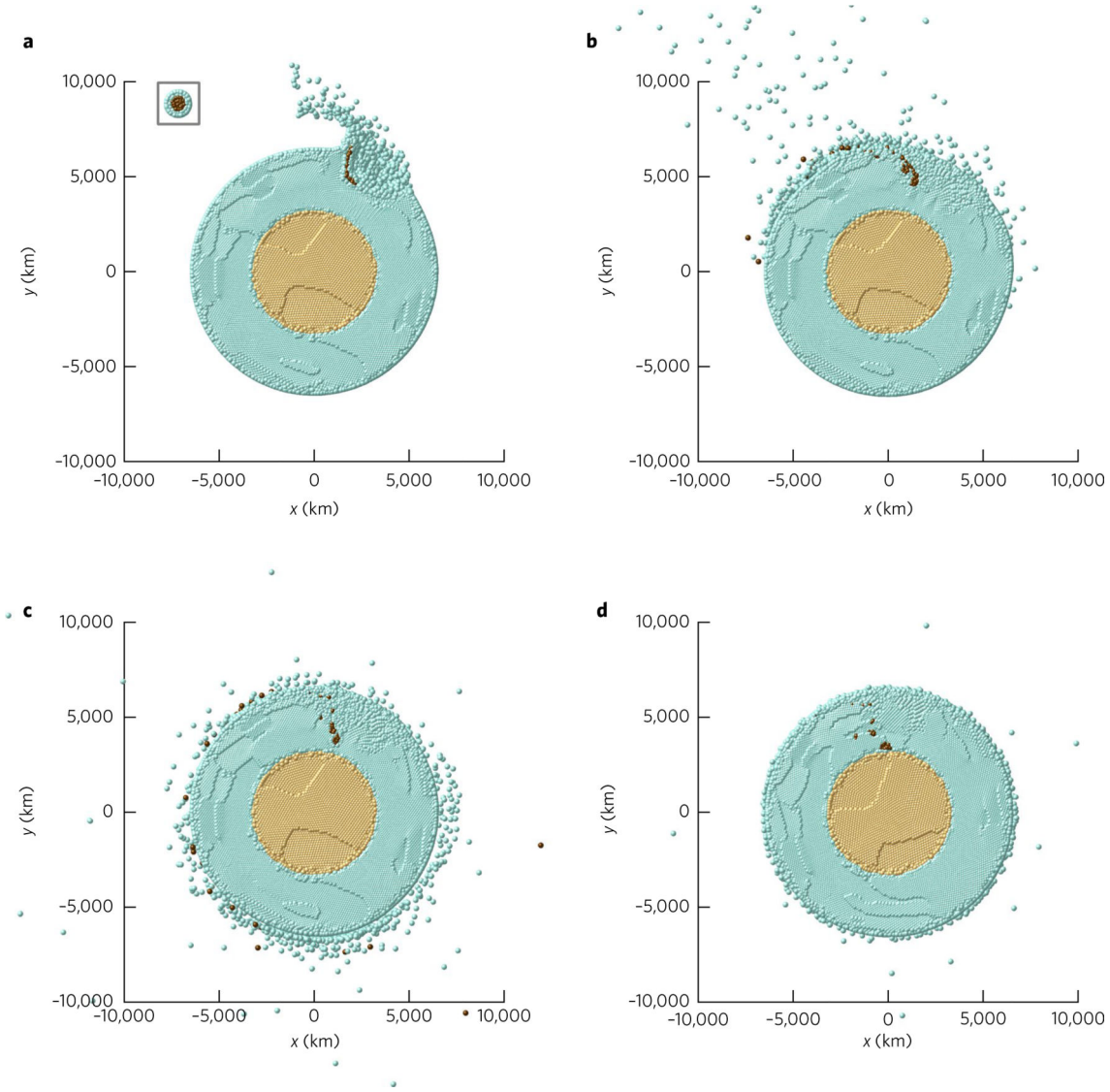

Fig. 1 |. Projectile's core interaction during large terrestrial collisions.

a–**d**, Four time steps in an SPH simulation (at 0.22 h (**a**), 0.97 h (**b**), 2.70 h (**c**) and 23.1 h (**d**)), with $M_i = 0.001\ M_{\oplus}$, (~1,400-km-diameter projectile), $\xi = 45°$ and $v_i/v_e = 1.7$. The green particles represent silicate material (Earth and projectile), the light brown particles indicate Earth's core and the dark brown particles indicate the projectile's core. The projectile size is shown for reference in the top-left corner of **a**.

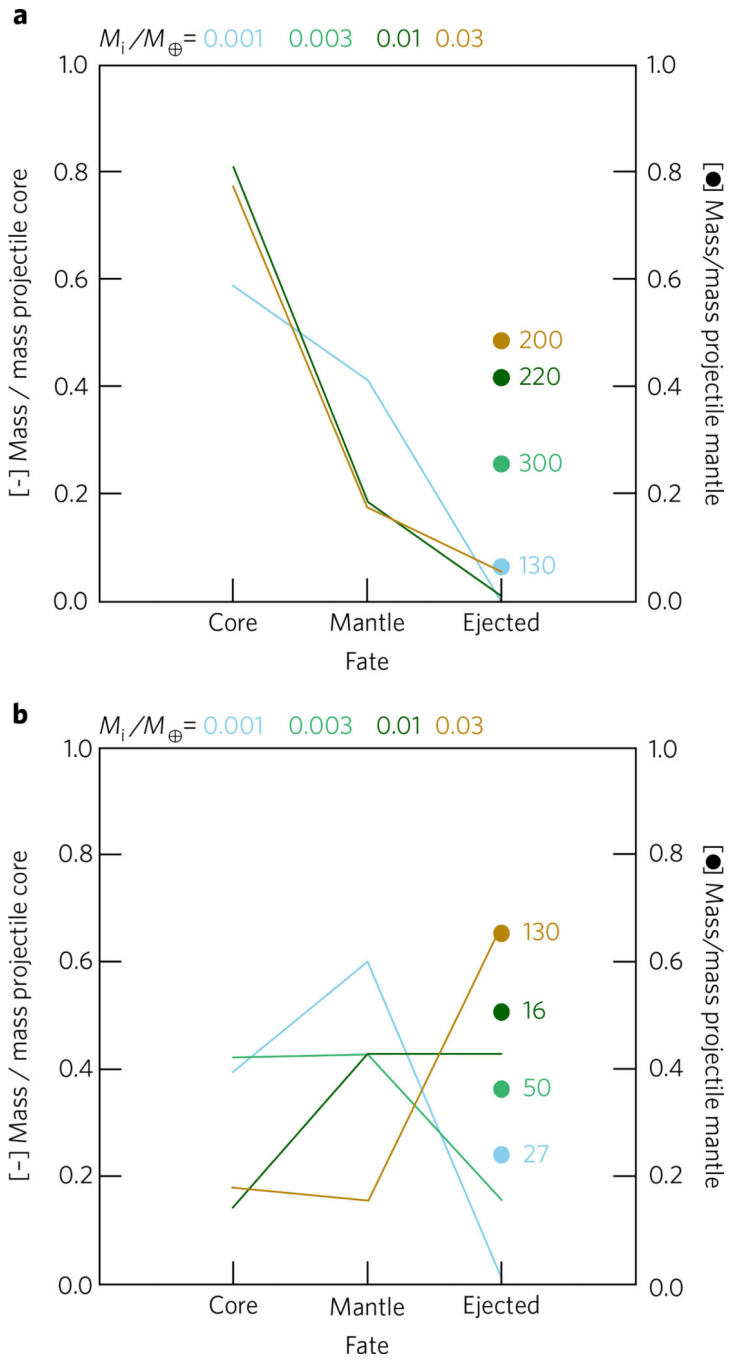

Fig. 2 |. Post-impact distribution of projectile material.

The *x* axis shows the fate of projectile material at the end of the SPH simulations (see text). The left-hand *y* axis indicates the normalized mass of the projectile's core in each location. Projectile masses as indicated: $\xi = 30°$ (**a**), $\xi = 45°$ (**b**). All cases have $v_i/v_e = 1.7$. Projectile mantle particles are assumed to be mixed with the Earth's mantle unless they are ejected from the system; the latter is indicated by the large dots and the right-hand *y* axis. The numbers next to the dots show $\delta M_t(\%)$ (see text). Note that in **a** the case $M_i/M_\oplus = 0.003$ is indistinguishable from $M_i/M_\oplus = 0.01$.

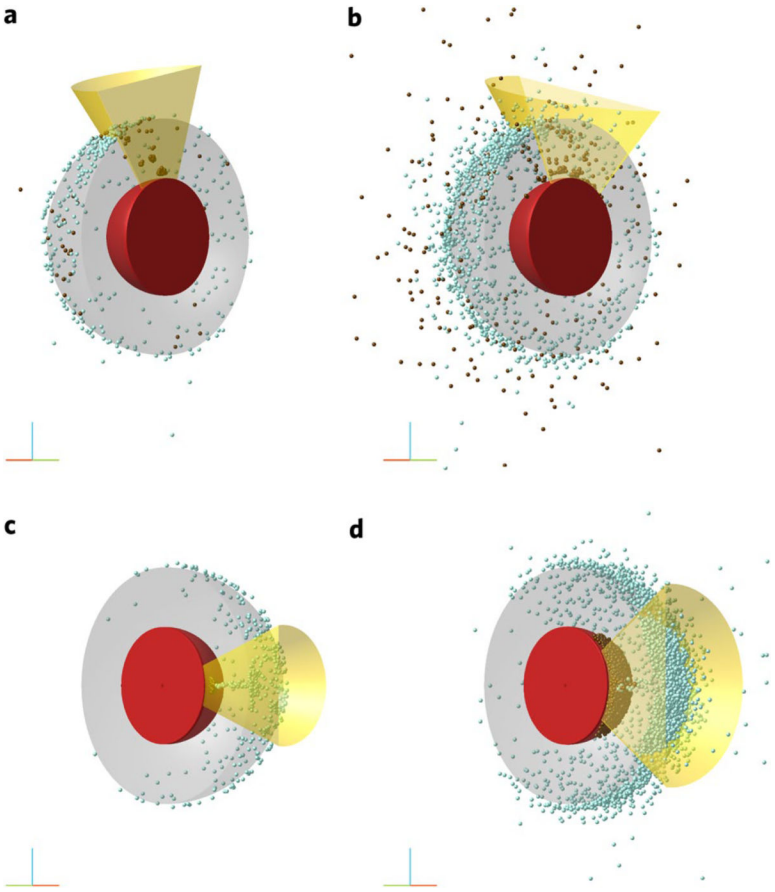

Fig. 3 |. Collisionally driven compositional heterogeneities.

a–**d**, Diagrams showing the location of the projectile's core (dark brown) and mantle (green) particles. Earth's particles are not shown for clarity, while the red and grey half-spheres indicate the Earth's core and surface, respectively. The simulations correspond to $M_i/M_\oplus$ = 0.001 (**a**), 0.03 (**b**), 0.001 (**c**) and 0.03 (**d**); impact angles of ξ = 45° (**a**,**b**) and 0° (**c**,**d**); v_i/v_e = 1.7 (**a**,**b**) and 1.2 (**c**,**d**). The yellow cones define regions of projectile material concentrations. The cone semi-aperture is 25° (**a**), 35° (**b**,**d**) and 20° (**c**). The orientation vectors are shown at the lower-left corner of each panel: *x* axis (red), *y* axis (blue), *z* axis (green).

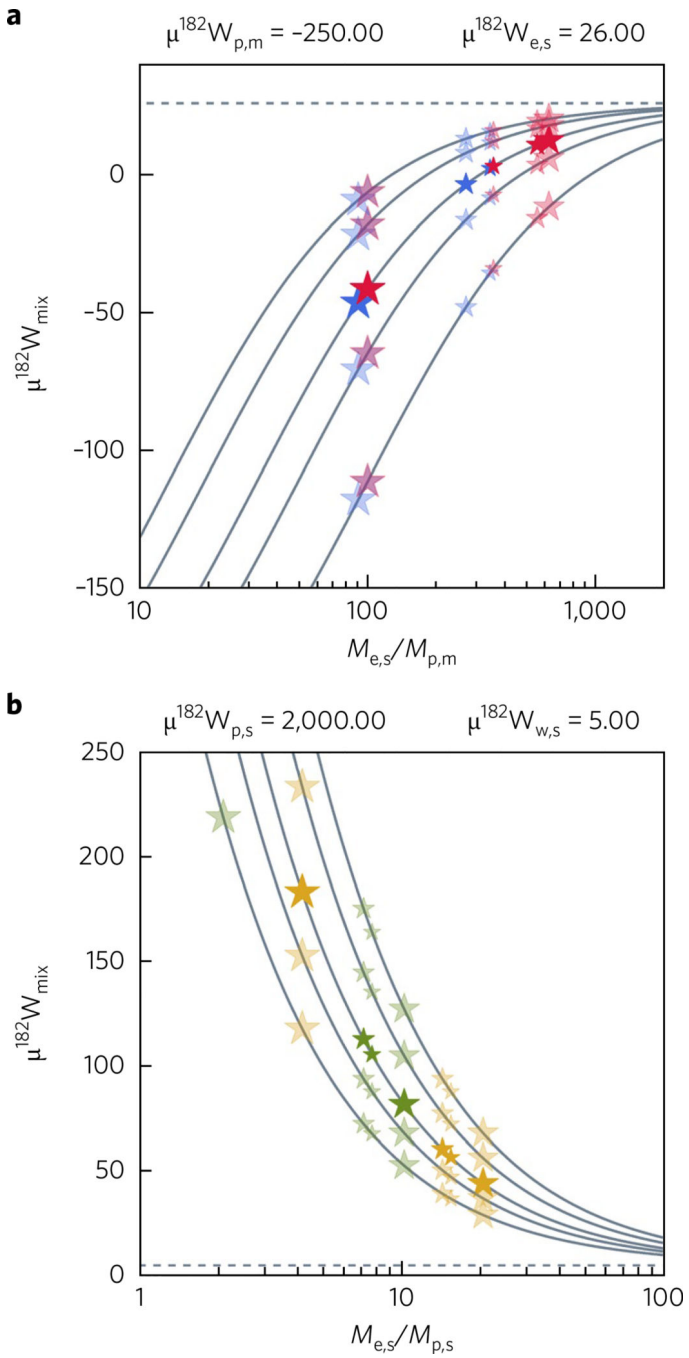

Fig. 4 |. Impact-driven W isotopic anomalies.

a, Negative $\mu^{182}W$ anomalies (in ppm) due to the addition of projectile core material of mass $M_{p,m}$ to domains in Earth's mantle of mass $M_{e,s}$. Curves correspond to mixing lines for constant absolute W ratios of the two components $W_{e,s}/(W_{e,s} + W_{p,m})$ = 1%, 2%, 3%, 5% and 7% (Methods). The stars indicate SPH simulations for ξ = 30° (red) and 45° (blue), with solid colour stars for $W_{e,s}/(W_{e,s} + W_{p,m})$ = 3%, our nominal model (Methods). The star size is proportional to the projectile mass ($M_i/M_\oplus$ = 0.001, 0.003, 0.01 and 0.03). The horizontal dashed line indicates an estimated pre-late accretion value for the silicate Earth of $\mu^{182}W_{e,s}$

= + 26 (Methods). **b**, Positive $\mu^{182}W$ anomalies due to the addition of projectile mantle material (subscript p,s) to near-surface spherical caps (subscript e,s). The curves correspond to mixing lines for constant absolute W ratios of the two components $W_{e,s}/(W_{e,s} + W_{p,s})$ = 60, 65, 71, 75 and 80% (Methods). The stars indicate SPH simulations for $\xi = 0°$ (green) and 30° (yellow), with solid colour stars for $W_{e,s}/(W_{e,s} + W_{p,s})$ = 71%, our nominal model (Methods). The star sizes and horizontal line are as in **a**. Here $\mu^{182}W_{e,s}$ = +5, corresponding to conditions during the late accretion epoch (Methods). A subset of simulations shown in these plots correspond to those in Fig. 3.